Radial localization of magnetospheric guided poloidal Pc 4-5 waves

R. E. Denton,[1] M. R. Lessard,[2] and L. M. Kistler[3]

Received 11 September 2002; revised 15 November 2002; accepted 26 December 2002; published 11 March 2003.

[1] The toroidal Alfvén wave, with magnetic field oscillations in the azimuthal direction, exhibits a singularity in the vicinity of the toroidal resonant frequency (field line resonance), so it is not surprising that this wave often exhibits varying frequency as a function of L shell. It is less clear why the poloidal Alfvén wave, with magnetic field oscillations in the radial direction, often exhibits a relatively constant frequency over a range of L shells. So far, the most promising proposal to explain this phenomenon is the theory of *Vetoulis and Chen* [1994, 1996], who showed that an energetically trapped global poloidal mode can exist in a region where the poloidal Alfvén frequency is lower than the toroidal frequency and where it exhibits a dip (minimum) with respect to L. While this theory is mathematically plausible, it has never been shown that poloidal Alfvén waves actually occur in association with such a dip in poloidal frequency. Here we examine poloidal wave events observed by the AMPTE/IRM spacecraft and calculate the theoretical poloidal frequency as a function of L using the equilibrium parameters obtained from the spacecraft observations. We find that the poloidal Alfvén wave does occur in association with such a dip (or at least a flattening) in poloidal frequency. While Vetoulis and Chen hypothesized that such a dip would occur because of a sharp gradient in plasma pressure, we find that the dip in poloidal frequency may result from the L dependence of the equilibrium density or magnetic field. The observed frequencies are in rough agreement with the theoretical frequencies, though in some cases we must assume that the observed oscillations result from a high harmonic (third or fourth harmonic structure along the magnetic field). We also apply the same analysis to compressional wave events (with oscillations in the direction of the equilibrium magnetic field). Such oscillations may be on the poloidal wave branch or the mirror mode branch. Here also, the observed fluctuations occur in the region of a dip in poloidal frequency. In one case the observed frequency is consistent with the theoretical poloidal frequency, whereas in another case it is not. *INDEX TERMS:* 2752 Magnetospheric Physics: MHD waves and instabilities; 2730 Magnetospheric Physics: Magnetosphere—inner; 2740 Magnetospheric Physics: Magnetospheric configuration and dynamics; 7871 Space Plasma Physics: Waves and instabilities; *KEYWORDS:* guided poloidal mode, Alfven wave, ULF wave, Pc 4-5

Citation: Denton, R. E., M. R. Lessard, and L. M. Kistler, Radial localization of magnetospheric guided poloidal Pc 4-5 waves, *J. Geophys. Res.*, *108*(A3), 1105, doi:10.1029/2002JA009679, 2003.

1. Introduction

[2] The magnetosphere often exhibits magnetic fluctuations in the radial, azimuthal, or parallel (to the direction of the background magnetic field **B**) direction. Depending on which of these components is dominant, the wave is termed the poloidal, toroidal, or compressional mode, respectively. Here we are most interested in the poloidal and compressional modes, particularly those which are internally driven by kinetic instability of ring current ions in the dusk local time sector [*Anderson*, 1993]. Poloidal and compressional fluctuations may result from the fast/magnetosonic mode; this mode is distinguished by density and pressure fluctuations which are in phase with the magnetic fluctuations. In contrast (in order that they not excite the fast/magnetosonic mode), low-frequency instabilities such as Alfvén waves must preserve pressure balance by having pressure and magnetic fluctuations which are out of phase.

[3] At plasma $\beta = 8\pi p/B^2$ small in comparison with unity (where p is the equilibrium pressure), the likely driving mechanism for poloidal fluctuations is the drift bounce resonant instability, a resonant instability driven by the hot ion pressure gradient and curvature [*Southwood*, 1976;

[1]Department of Physics and Astronomy, Dartmouth College, Hanover, New Hampshire, USA.
[2]Thayer School of Engineering, Dartmouth College, Hanover, New Hampshire, USA.
[3]Space Science Center, University of New Hampshire, Durham, New Hampshire, USA.

0148-0227/03/2002JA009679$09.00

Chen and Hasegawa, 1988, 1991; *Chan*, 1991]. At β of order unity the waves may be driven by the drift bounce resonant instability or by the drift mirror mode, which is driven by temperature anisotropy [*Cheng and Lin*, 1987; *Chen and Hasegawa*, 1991]. Actually, the two modes are coupled, especially at high β. For both modes, the high-β waves will have a large compressional component (along $\hat{\boldsymbol{b}}$). These theories predict that the fundamental mode (no node in azimuthal electric field) will be stable and that the most unstable mode will have second harmonic structure along the magnetic field (single node in azimuthal electric field at the equator) [*Cheng and Lin*, 1987; *Chen and Hasegawa*, 1988, 1991; *Cheng and Qian*, 1994].

[4] The kinetic instabilities are generally most unstable when the azimuthal wavelength is of the order of the proton gyroradius. Since the driving population is expected to be the ring current with energy $\sim$100 keV, the dominant unstable waves have small azimuthal wavelength compared with the radial distance to the wave region LR_E, where R_E is the Earth radius. This leads to the growth of a wave with large azimuthal mode number $m = k_\phi LR_E \sim 100$, where k_ϕ is the azimuthal wave number. It is easy to see from $\nabla \cdot \boldsymbol{\delta B} = 0$ that the character of the Alfvén mode must change depending on m; for small m, the Alfvén mode will be dominantly toroidal, whereas for large m, it will be dominantly poloidal.

[5] A remarkable feature of the internally driven (with out of phase pressure and magnetic fluctuations) poloidal and compressional waves is that they may be nearly monochromatic over a range of L shell [e.g., *Takahashi et al.*, 1987]. In the inhomogeneous magnetosphere one would normally expect that the wave frequency would decrease with respect to L. In fact, this normally occurs for the continuum of toroidal Alfvén waves that is observed in the magnetosphere [*Takahashi et al.*, 2002]. With such variation of frequency, the natural tendency of the Alfvén wave is to break up via phase mixing into more and more radial structure until the radial wave vector $k_r > k_\phi$ so that the wave is dominantly toroidal [*Ding et al.*, 1995; *Mann and Wright*, 1995].

[6] So what can then allow the poloidal mode to be quasi-monochromatic over a range of L? Dissipative effects such as ionospheric resistivity and/or ion gyroradius effects are sometimes invoked to give a finite mode width, but there will still be eigenmodes centered about each L shell, and phase mixing of these finite width modes will still occur. If the poloidal Alfvén frequency happens to be flat with respect to L in some region of L, then the poloidal mode could have a finite width there, though in that case the energy would not be expected to be confined (L. Chen, private communication, 2001). Probably the most promising explanation for the global structure of the poloidal mode is the theory of *Vetoulis and Chen* [1994, 1996]. They showed that an energetically trapped global poloidal mode can exist in a region in which the poloidal frequency is below the toroidal frequency and in which there is a dip (minimum) in the poloidal mode frequency with respect to L. The frequency of this mode would be above the minimum in frequency but still within the values of lowered frequency (within the dip). Energy will gradually leak out of this region to be absorbed at the toroidal resonance, but if the dip is large enough that leakage will be slow [*Denton and Vetoulis*, 1998].

[7] In this paper we calculate the poloidal Alfvén frequency as a function of L based on the observed equilibrium profiles for several poloidal and compressional wave events observed by the AMPTE/IRM spacecraft. In section 2 we describe our dataset and method, while in section 3 we present our results. We end with discussion and a summary in section 4. Our calculations are based on the MHD poloidal mode frequency, which is clearly relevant only for radially polarized waves. Observed compressional mode frequencies may or may not be related to the poloidal frequency. If the compressional mode is a high beta version of the poloidal mode, the frequency of the observed wave is expected to be similar. On the other hand, compressional waves may be on the compressional (mirror mode) branch, leading to entirely different dispersion (F. Cheng, private communication, 2001).

2. Data and Method

[8] The AMPTE/IRM spacecraft, operated from August 1984 to August 1986, had an apogee of 18.8 R_E, a perigee of 552 km, an inclination of 28.7° to the equatorial plane, and an orbital period of 44.3 hours. For the events discussed in this paper, IRM is near the magnetic equator at magnetic latitude MLAT ranging from -16 to $-6°$. IRM plasma and magnetic field data have been obtained from the University of New Hampshire at approximately 5 s resolution. Descriptions of the plasma instrument and magnetometer are given by *Paschmann et al.* [1985] and *Lühr et al.* [1985], respectively. The plasma instrument is used only to obtain the plasma pressure. It detects ions up to energy 40 keV. When available, we add the pressure for ions with energy >40 keV obtained from the SULEICA experiment [*Möbius et al.*, 1985].

[9] The electron density is obtained from the upper hybrid noise band measured using the plasma wave instrument [*Häusler et al.*, 1985]. We normally measured the upper hybrid frequency as the midpoint of the upper hybrid noise band. While at least 10 s resolution is available, we normally computed the density with $1-5$ min resolution using higher resolution when needed. Since IRM has no ion composition information, we assumed the ion measurements to be predominantly due to protons (see *Paschmann et al.* [1986] and *Li et al.* [1995] for a discussion of the error involved). The equilibrium quantities (magnetic field, density, and pressure) are averaged over at least 5 min.

[10] In order to compute the poloidal Alfvén mode frequency with respect to L shell, we need the equilibrium plasma parameters in a meridional plane (assuming azimuthal symmetry). Assuming that the magnetosphere is roughly in equilibrium, we first obtain the equilibrium parameters on a radial cut corresponding to the trajectory of the IRM spacecraft. To get the parameters along the equatorial plane, the density and scalar pressure are mapped from the spacecraft position to the equator along dipole field lines, and the magnetic field is mapped assuming that the amplitude of the field varies as in the dipole field model. We then use two methods to generate a two-dimensional (meridional plane) equilibrium for our computations. The first is not a true equilibrium. We calculate the magnetic flux radially outward along the equator and then map that flux down to the ionosphere (assumed to be perfectly conducting

at a radius of $1.15R_E$) along dipole field lines, letting the flux be constant along these lines. From the flux we can calculate the magnetic field on each field line. We set the pressure equal to a constant along each dipole field line, and the density is assumed to vary like $R^{-1.5}$ off the equator along field lines [*Goldstein et al.*, 2001]. We call this the mapped dipole equilibrium. Note that although the shape of the field lines is dipolar (since the flux is constant along dipole field lines), the value of B along these field lines is not consistent with a simple dipole field model (since the equatorial flux is not that of a simple dipole field).

[11] The second method for generating an equilibrium employs a two-dimensional MHD simulation in the meridional plane. The parameters in the region of interest are initially set up as described previously (for the non self-consistent equilibrium) except that the density is chosen to make the Courant condition constant in the entire simulation domain (so large time steps can be used in the simulation; the density does not affect equilibrium, and it is reset to realistic values later). The inner L shell boundary of the simulation is at low enough L that the plasma beta is small, and the inner boundary can be assumed to be dipolar. The outer boundary is also dipolar, not a realistic assumption, but the outer L is made large enough so that the outer boundary does not greatly influence the region of interest. For instance, for our first event we are interested in the region $7.5 \leq L \leq 9.2$ (see Figure 2). The inner and outer L values for the simulation are chosen to be 5.5 and 14.0, respectively. In L shells beyond the region of interest we set the pressure to a constant (the value at the outermost L of the region of interest, chosen if possible where the pressure gradient is flat) and vary the magnetic flux along the equatorial plane according to the dipole field model (so that the outer region is initially in equilibrium). We then run the MHD simulation, using a large viscosity, and zeroing the plasma velocity in the entire simulation domain every time the kinetic energy reaches a maximum value. In this way we generate a true MHD equilibrium, after which we reset the density to the original values as a function of magnetic flux.

[12] The question naturally arises as to which equilibrium, the mapped dipole or the MHD equilibrium, is the most realistic. The MHD equilibrium is a true equilibrium; however, the MHD simulation may smear out the gradients in the original equilibrium parameters. In our view the most realistic equilibrium may be something in between our two numerical equilibrium models. The best confirmation that our equilibrium parameters are reasonable is if the two model equilibria agree.

[13] Once we have an equilibrium, we can solve for the poloidal mode eigenfrequency using (equation (6) of *Denton* [1998] or equation (12) of *Vetoulis and Chen* [1996])

$$\left[\frac{1}{B}\partial_l \frac{|\nabla\phi|^2}{B}\partial_l + \frac{\omega^2|\nabla\phi|^2}{V_A^2 B^2} + 2\frac{\kappa_\psi}{B^2}\partial_\psi p\right]\eta_\phi = 0, \qquad (1)$$

where the nonorthogonal coordinates are the azimuthal angle ϕ, the magnetic flux ψ, and the distance along a field line from the equator l. The equilibrium magnetic field is $\boldsymbol{B} = \nabla\phi \times \nabla\psi$, the perturbed vector potential is $\boldsymbol{\eta} = \eta_\phi\nabla\phi + \eta_\psi\nabla\psi$ with $\boldsymbol{E} = -\partial_t\boldsymbol{\eta}$, the Alfvén speed is $V_A = B/\sqrt{4\pi\rho}$, the mass density is ρ, and $\kappa_\psi \equiv (\boldsymbol{\kappa}\cdot\nabla\psi)/|\nabla\psi|^2$, where $\boldsymbol{\kappa}$ is the curvature, and ω is the wave angular frequency. Schematically (ignoring geometrical factors), this equation is equivalent to

$$\left[k_\parallel^2 + \frac{\omega^2}{V_A^2} - \frac{2}{R_C B^2}\frac{\partial p}{\partial(LR_E)}\right]\delta E_\phi = 0, \qquad (2)$$

where $k_\parallel$ is the component of the wave vector along the magnetic field, and R_c is the radius of curvature. For both the mapped dipole and MHD equilibrium models the full model variations of $\boldsymbol{B}$ and $\boldsymbol{\kappa}$ along field lines are included in the calculations using equation (1).

[14] The toroidal mode (azimuthal fluctuations in the magnetic field) eigenmode equation is given in equation (8) of *Denton and Vetoulis* [1998] (see also *Vetoulis and Chen* [1996]). A schematic equation for the toroidal mode would look just like equation (2), except that E_ϕ would be replaced by E_L (''radial'' component) and the pressure gradient term (last term in the square bracket) would be absent.

3. Wave Events

3.1. 4 June 1985 Event

[15] A poloidal mode event was observed on 4 June 1985, 2100–2150 UT. The location in SM coordinates was R = 8.6 R_E, MLAT = −6.7°, and MLT = 18.5 hours. Thus this event (as well as the others discussed in this paper) occurred at dusk, where events driven by the energetic ring current are most likely. No fluctuations in the solar wind magnetic field were evident at this time (not shown; solar wind plasma data were not available). Also, no corresponding oscillations were observed in the data from the Greenland Magnetometer Chain at MLT = 19.4, 0.9 hours east of IRM (not shown).

[16] Figures 1a–1c show the three components of the perturbed magnetic field $\delta\boldsymbol{B}$ plotted versus time for the 4 June 1985 poloidal mode event during the time that the wave amplitude was greatest. The coordinate system is field aligned, where the $\hat{z}$ direction is that of the equilibrium magnetic field $\boldsymbol{B}$, $\hat{\boldsymbol{y}} = \hat{z} \times \hat{\boldsymbol{r}}$ where $\hat{\boldsymbol{r}}$ is the geocentric radial direction to the spacecraft position ($\hat{\boldsymbol{y}}$ is roughly the azimuthal direction), and $\hat{\boldsymbol{x}} = \hat{\boldsymbol{y}} \times \hat{z}$ (roughly the L direction, which we will loosely refer to as ''radial''). Note that the perturbed magnetic field is transverse (z component small) and that the dominant component is δB_x, which indicates that this is a poloidal mode (radial component dominant). Figure 1d shows that the perturbed magnetic field amplitude δB (thin curve) and the perturbed pressure δp (thick curve) are out of phase as we would expect for a low-frequency Alfvén wave (and contrary to expectations for the fast/magnetosonic mode).

[17] Figures 2a–2c also show δB_x, δB_y, and δB_z for the same event (4 June 1985, 2100–2150 UT) but now plotted versus L. The notation ''180'' above Figure 2a indicates that δB and δp are 180° out of phase (Figure 1d), and the horizontal line directly above roughly indicates the period of wave activity as a function of L. Note that the mode frequency is nearly constant over a rather large range of L (8–9).

[18] Figures 2d–2g show the equilibrium parameters. SULEICA [*Möbius et al.*, 1985] data were available for

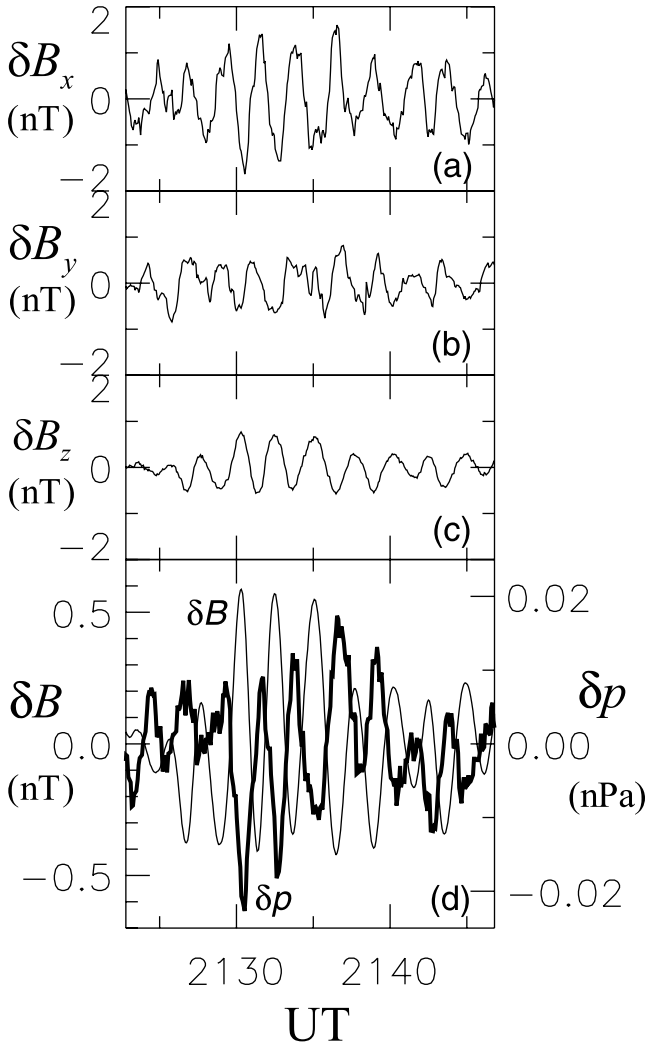

Figure 1. Perturbed magnetic field components (a) δB_x, (b) δB_y, and (c) δB_z, and (d) perturbed magnetic field amplitude δB (thin curve) and pressure δp (thick curve), all versus time, for the poloidal mode event observed on 4 June 1985, 2100–2150 UT.

this event. Although the high-energy contribution to the total pressure is not great, this component contributes a relatively greater amount to the pressure gradient because of a steeper falloff with respect to L. The solid curves show the parameters based on the measured data (mapped dipole

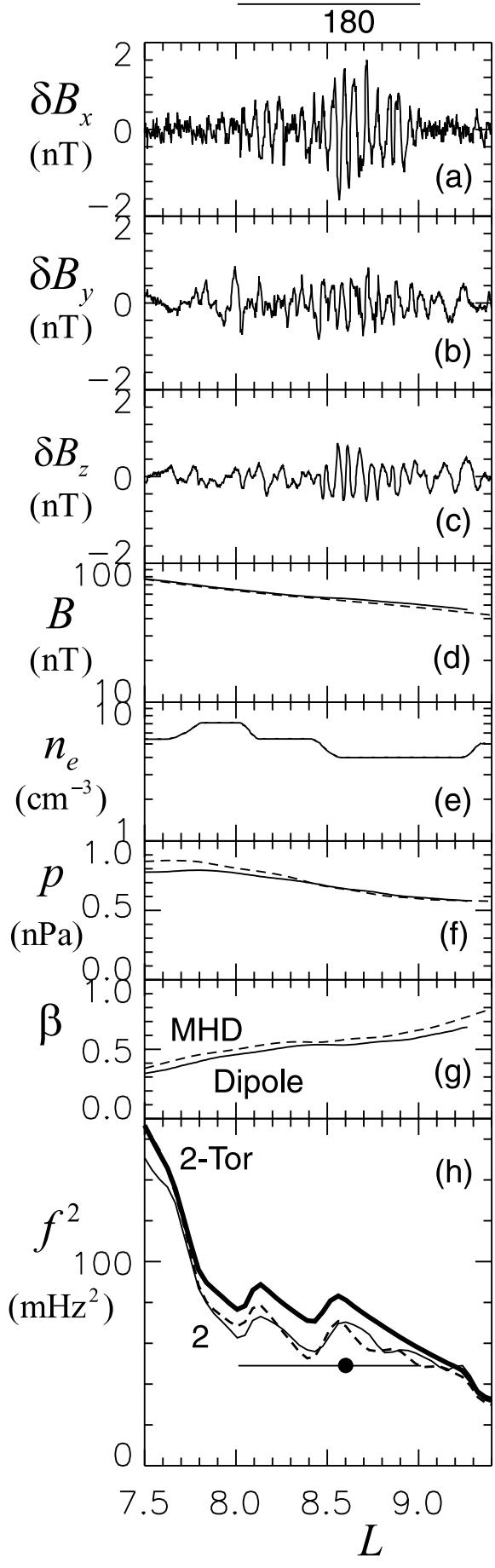

Figure 2. (opposite) For the poloidal mode event observed on 4 June 1985, 2100–2150 UT, the perturbed magnetic field components (a) δB_x, (b) δB_y, and (c) δB_z, the equilibrium (d) magnetic field B, (e) electron density n_e, (f) pressure p, and (g) plasma beta β, and the (h) squared frequency f^2 for the poloidal (thin curves) and toroidal (thick curve) mode. The filled circle is plotted at the L value for which the poloidal mode amplitude is a maximum and the superimposed horizontal line indicates the range of L over which the poloidal mode is observed. In Figures 2d–2h the solid and dashed curves are for the mapped dipole and MHD equilibria, respectively.

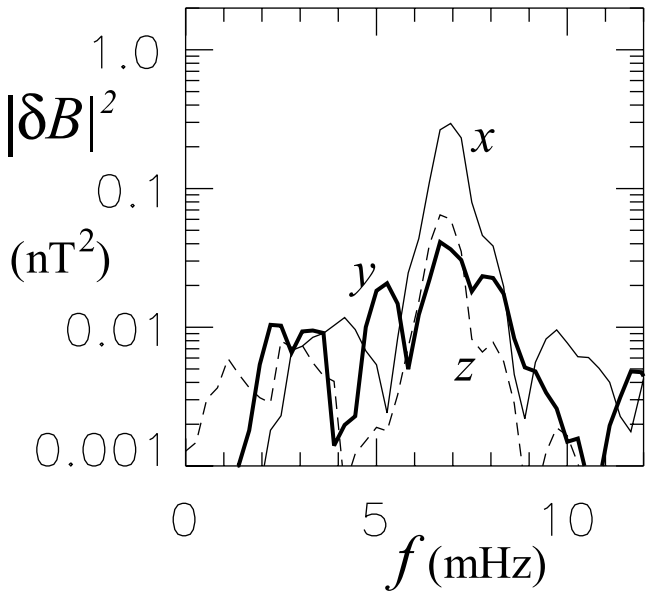

Figure 3. Power spectrum of the perturbed magnetic field components δB_x (thin solid), δB_y (thick solid), and δB_z (thin dashed), versus frequency f for the poloidal mode event observed on 4 June 1985, 2100–2150 UT.

equilibrium model), while the dashed curves show the parameters evolved in the MHD simulation. In this case the parameters from both equilibrium models agree fairly closely, which indicates that the equilibrium parameters are fairly reliable. In Figure 2h we plot the squared frequency f^2 in mHz^2 for the poloidal mode (thin curves) and toroidal mode (thick curve) of the second harmonic (which is most likely to be unstable; see references in section 1). The thin solid curve is based on the parameters from the mapped dipole equilibrium model, while the dashed curve is based on the evolved parameters from the MHD simulation. Again, these values are fairly close.

[19] As we have already noted, the polarization and δB-δp phase relation are consistent with the poloidal mode. Further support for this identification is provided by the observed wave frequency. Figure 3 shows the power spectrum of the perturbed magnetic field components δB_x (thin solid), δB_y (thick solid), and δB_z (thin dashed), versus frequency f. The dominant power is in the poloidal (δB_x) component at 7 mHz. The square of this frequency is also plotted in Figure 2h as a filled circle. This circle is plotted at the L shell corresponding to the largest amplitude of the wave (L = 8.6), and the superimposed horizontal line indicates the extent of the region over which the mode is observed ($8.0 \leq L \leq 9.0$). It is clear that the theoretical poloidal mode frequencies (thin curves) are fairly close to the observed frequency (filled circle and horizontal solid line). Note also from Figure 2f that $\partial p/\partial L < 0$ (inward pressure gradient), and from equation (2) that the pressure gradient leads to a reduction in the poloidal mode frequency $f = \omega/(2\pi)$ relative to that of the toroidal mode. This effect can be seen in Figure 2h, which shows that the poloidal mode frequency (thin curves) is lower than the toroidal mode frequency (thick curve).

[20] On the basis of the theory of *Vetoulis and Chen* [1994, 1996] we would expect to find the poloidal mode in a region where the poloidal frequency is less than the toroidal frequency (which is the case) and where there is a dip in the poloidal frequency with respect to L. There are in fact two small dips in poloidal frequency, a smaller one at L = 7.9–8.1 and the larger at 8.2–8.6. These dips occur predominantly because of sharp changes in the density profile n_e rather than because of a sharp drop in pressure as hypothesized by *Vetoulis and Chen* [1994, 1996]. However, the pressure gradient does play an important role; it causes the poloidal frequency to be below the toroidal frequency (which is also required by Vetoulis and Chen's theory). While the alignment is not perfect, we note that the envelope of the magnetic field oscillations (Figure 2a) exhibits two peaks at about L = 8.15 and 8.65, which are very close to the dips in poloidal frequency. If there were exact agreement with the theory, the observed frequencies would be above the minima in the theoretical frequency; this is not the case, but these frequencies are definitely close to each other.

3.2. 26 July 1986 Event

[21] Three wave events occurred on 26 July 1986, during 1500–1800 UT. At 1700 UT, IRM's location was R = 8.5 R_E, MLAT = −15.6°, and MLT = 16.8 hours. SULEICA data were also available for this time period. Figure 4 summarizes our results for these three events. The first of these is poloidal (δB_x dominant), and occurs at L = 6.8–8.0 under the notation "180?" at the top of the figure. This notation indicates that δB and δp are approximately out of phase, though the phase relation between these quantities is not completely consistent. (As discussed earlier, we use this phase relation to rule out the possibility that the waves are a fast/magnetosonic mode.) The second and third wave events have a very consistent 180° phase difference between δB and δp. Under the left "180" notation, at L = 8.5–9.8, there is a large amplitude compressional event (δB_z dominant). Oscillations with similar frequency were observed by the EISCAT magnetometer chain (not shown) at MLT = 20 (3 hr east of IRM). Under the rightmost "180" notation, at L = 9.8–10.2, there is a relatively high frequency poloidal oscillation. An arrow in Figure 4a indicates the exact position of this oscillation (with about 6 wave periods).

[22] The equilibrium magnetic field from the MHD simulation (Figure 4d) is fairly close to that of the observed parameters (mapped dipole model). There is a greater difference in the equilibrium pressure profiles (Figure 4f), though the equilibrium beta values are fairly similar except for a slight shift in L (Figure 4g). Unfortunately, the IRM plasma wave instrument [*Häusler et al.*, 1985] did not give reliable data except when the spacecraft was at L = 9.2–10.1 (L range of solid curve in Figure 4e). For both the mapped dipole and MHD equilibrium models, we used a $n_e \propto L^{-4.5}$ fit (plasmatrough L dependence given by *Carpenter and Anderson*'s [1992] electron density model). This fit (dashed curve in Figure 4e) describes the L range of the observed density fairly well (Figure 4e), and may be adequate to model the compressional and second poloidal event. However, it is clear that our extrapolation of density to L = 7–8 (where the first poloidal event occurs), though reasonable, is very uncertain.

[23] In Figure 4h, the lowest three curves correspond to the same curves plotted in Figure 2h. The thick solid curve

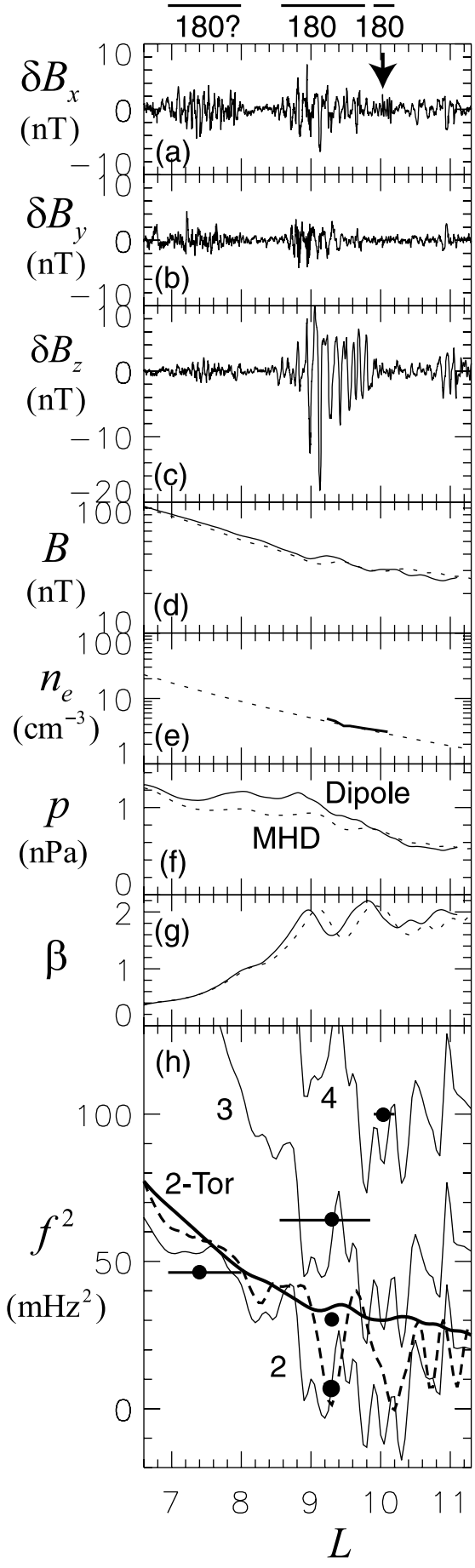

indicates the squared frequency of the second harmonic of the toroidal mode, and the other two curves indicate the squared frequency of the second harmonic of the poloidal mode using the equilibrium parameters from the observations (thin solid curve) and the MHD simulation (thin dashed curve). The curves marked "3" and "4" are for the third and fourth harmonic poloidal mode using the observed equilibrium parameters (mapped dipole model). One filled circle is plotted at the position of the square of the observed frequency for the two poloidal events (L = 7.3 and 10.1). For the compressional event (L = 9.3) there are three harmonics with significant wave power, and a filled circle is plotted at the squared frequency corresponding to each of these. For each of these waves events, we have plotted a horizontal line segment indicating the rough L range of the event. (For the compressional event, this horizontal line is drawn at the filled circle corresponding to the highest frequency harmonic only, that is, at the highest of the three filled circles.)

[24] If the observed parameters are used (mapped dipole equilibrium model), the first poloidal event (leftmost filled circle and horizontal line in Figure 4h) occurs in the region of a very small dip in the squared poloidal frequency of the second harmonic (lowest thin solid curve in Figure 4h). With the equilibrium from the MHD simulation (dashed curve), there is no longer a dip in the frequency, though the frequency does become slightly flatter there. The theoretical and observed frequencies agree fairly well for this event, though we must keep in mind the significant uncertainty related to the lack of observed density in this region.

[25] The compressional event (L = 8.5–9.8) occurs in the region of a very large dip in the squared frequency of the poloidal mode for both equilibrium models (lowest thin solid and dashed curves) with the squared frequencies of all harmonics above the lowest theoretical frequency. In this case the theoretical squared frequency of the poloidal mode becomes negative using the observed parameters, indicating that the mode is ballooning unstable. (Ballooning instability would certainly lead to large oscillations as are observed. However, even if the plasma is not ballooning unstable but is near to ballooning instability, resonant effects will likely lead to a large growth rate.) As mentioned earlier, there is some uncertainty as to whether the compressional mode frequency is on the poloidal mode or mirror mode dispersion surface. If it is on the poloidal mode branch, the lowest two frequencies are consistent with the *Vetoulis and Chen* [1996] theory. The highest frequency harmonic might be

Figure 4. (opposite) Poloidal and compressional events observed on 26 July 1986, 1500–1800 UT, with the same format as Figure 2. The wave events occur under the "180?" and "180" markings at the top of the figure. These waves are poloidal (δB_x dominant) at L = 6.8–8.0 and L = 9.8–10.2, and compressional (δB_z dominant) at L = 8.5–9.8. In Figure 4h the lowest three curves are the same as those plotted in Figure 2h. The curves marked "3" and "4" are for the third and fourth harmonic poloidal mode using the observed equilibrium parameters (mapped dipole model). One filled circle is plotted at the square of the observed frequency for the two poloidal events. For the compressional event there are three filled circles (vertically arranged) for the three harmonics observed.

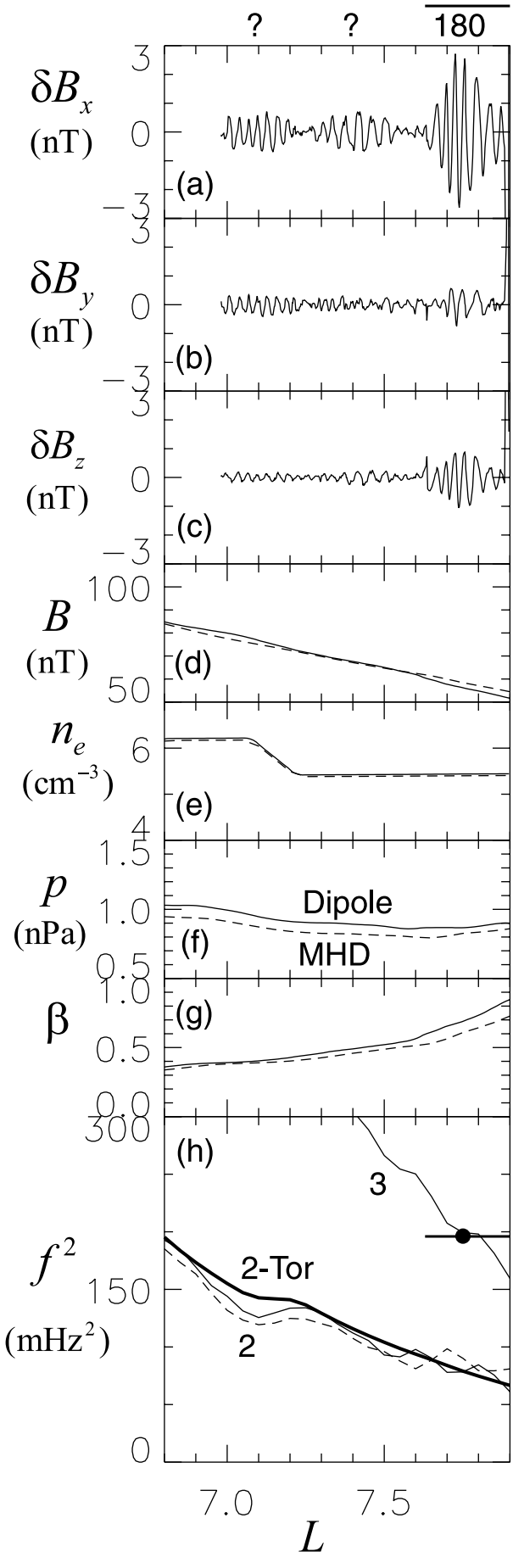

produced by nonlinear coupling. Alternately, the highest frequency component might have third harmonic parallel structure since the frequency of this harmonic matches the frequency of the theoretical third harmonic poloidal mode (curve marked "3 in Figure 4h). Similarly, the second poloidal event (L = 9.8–10.2) occurs at a dip in the squared poloidal frequency of the fourth harmonic (curve marked "4" in Figure 4h). It is possible that poloidal modes can occur with these higher harmonic field aligned structures (the harmonic number corresponds to one plus the number of nodes along the field line), and for these, the stabilization effect associated with the even fundamental mode [*Cheng and Lin*, 1987; *Chen and Hasegawa*, 1988, 1991; *Cheng and Qian*, 1994] does not have a strong effect (L. Chen, private communication, 2001).

3.3. 17 May 1985 Event

[26] Figure 5 shows a poloidal wave event observed on 17 May 1985, at UT 0951–1024. At 1020 UT, IRM's location was R = 7.7 R_E, MLAT = −5.8°, and MLT = 19.4 hours. Solar wind (IMP-8) data were available at this time, and there was no clear connection between these fluctuations and those in the solar wind. This wave event consisted of three wave packets. The first two of these (below the notation "?") did not have a consistent out of phase relationship between δB and δp. We cannot rule out the possibility that these are traveling fast/magnetosonic waves and we will not consider them further, except to note that they could be traveling waves produced at the location of the third wave packet. The third wave packet had a clear 180 degree phase relation between δB and δp. In this case the observed frequency matches that of the third harmonic of the poloidal mode (curve marked "3" in Figure 5h). The theoretical frequency has a slight flattening at that L value but not a dip. In this case the SULEICA data were not available, so we may not be measuring all the plasma pressure.

3.4. 6 June 1985 Event

[27] On 6 June 1985, at 1718–1900 UT, there was a large-amplitude, low-frequency compressional mode similar to that of the 26 July 1986 event. At 1818 UT, IRM's location was R = 9.2 R_E, MLAT = −6.8°, and MLT = 18.5 hours. Oscillations with similar frequency were observed by the EISCAT magnetometer chain (not shown) at MLT = 22 (3.5 hours east of IRM). There were no SULEICA data available for this event. The results of our analysis are shown in Figure 6. Because of a change in frequency, we considered two different periods of wave activity, that which occurred when the spacecraft was at L = 7.9–9.2, and when it was at L = 9.3–10.3 (see the horizontal lines in Figure 6h). In both cases, the compressional component (δB_z) was greatest (Figure 6a–6c). As indicated by the "180" notation above Figure 6a, there was a clear 180 degree phase relation between δB and δp for both of these time periods.

[28] The equilibrium parameters for this event differ somewhat depending on which model is used, the mapped dipole model using the observed parameters (solid curves in Figures 6d–6g) or the MHD simulation model (dashed

Figure 5. (opposite) Three poloidal wave packets observed on 17 May 1985, UT 0951–1024. The format is the same as that of Figure 4.

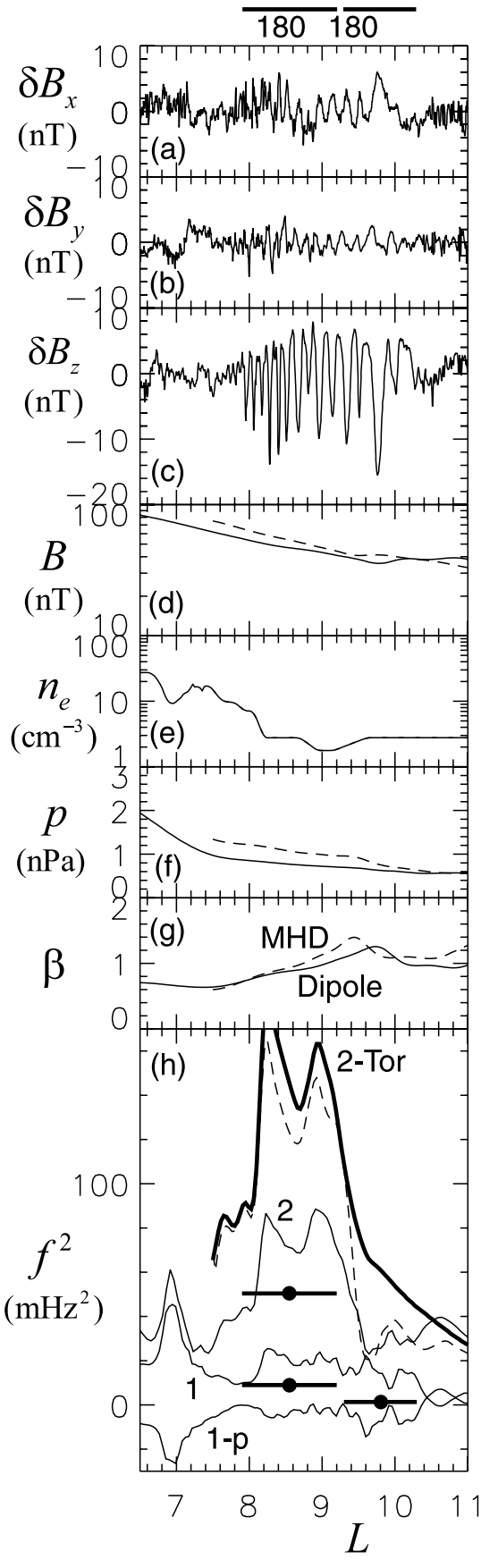

curves in Figures 6d–6g). In particular, the equilibrium magnetic field (Figure 6d) and pressure (Figure 6f) are somewhat higher in the MHD equilibrium, and the peak in plasma beta is closer to the Earth (Figure 6g).

[29] Figure 6h compares the observed frequencies to the theoretical ones. The top two curves (dashed and thick solid curves) are based on the MHD simulation model whereas the other curves are based on the mapped dipole model. The middle curve marked "2", the squared poloidal frequency based on the mapped dipole model, is significantly lower than the dashed curve based on the MHD model, mostly because of the difference in the equilibrium magnetic field. In the first period of wave activity we have drawn filled circles and horizontal lines at squared frequency values corresponding to two harmonics. The squared frequency of the higher harmonic is not a great distance off from the squared frequency of the poloidal mode based on the mapped dipole model (highest thin solid curve marked "2"), but the squared frequency of the lowest observed frequency (9 mHz^2) is much lower than the the squared theoretical second harmonic frequencies for both equilibrium models, and the same holds for the squared frequency of the observed wave in the second period of wave activity (1.3 mHz^2 at L = 9.3–10.3). The theoretical squared frequency for the fundamental poloidal mode is plotted in the two lowest curves of Figure 6h. The very lowest curve marked "1-p" is computed using the poloidal dispersion relation (1), which yields negative values indicating ballooning instability. However, as discussed in section 1, a better approximation may be to neglect the pressure term in equation (1); this yields the curve marked "1" in Figure 6h. As is clear from Figure 6h, the squared frequency of the observed low frequency waves agrees better with the theoretical fundamental mode squared frequencies than with the second harmonic squared frequencies. Possibly the fundamental mode could be excited owing to effects not included in the standard theories [see, e.g., *Mann and Chisham*, 2000]. However, there is no good agreement between the observed waves and any theoretical curves, including the fundamental, and as discussed earlier, this may indicate that the compressional oscillations correspond to a different wave branch. (Note added in proof: If the composition of the plasma is predominantly oxygen rather than hydrogen, the theoretical frequency marked "2" in Figure 6h would be consistent with the lowest observed harmonics indicated by the lowest filled circles in Figure 6h).

4. Discussion and Summary

[30] While it is not surprising that the toroidal mode (azimuthal oscillations of the magnetic field) oscillates with a well-defined frequency at a particular L shell (owing to the

Figure 6. (opposite) Compressional wave observed on 6 June 1985, 1718–1900 UT. The format is the same as that of Figure 4. The two lowest frequency curves in Figure 6h display the theoretical squared frequency for the fundamental poloidal mode. The curve marked "1-p" includes the pressure term in the eigenmode equation and is ballooning unstable (squared frequency <0). The curve marked "1" is calculated without the pressure term. The three higher frequency curves are the same as those in Figure 2.

field line resonance), it is still a mystery as to how the poloidal mode can oscillate with a relatively constant frequency over a range of L shell [*Takahashi et al.*, 1987]. *Vetoulis and Chen* [1994, 1996] showed that an energetically trapped poloidal mode can exist in a region in which the poloidal frequency is below the toroidal frequency and in which there is a dip in the poloidal mode frequency with respect to L. In order to test whether this mechanism actually occurs, we have calculated the theoretical poloidal frequency for four wave events observed by the AMPTE/IRM spacecraft and have compared it with observed poloidal and compressional wave frequencies. Compressional mode frequencies may or may not be related to the poloidal mode frequency depending on whether the compressional mode is on the poloidal or mirror mode dispersion surface.

[31] For two of the four wave events (4 June 1985 and 26 July 1986) we have high-energy (>40 keV) particle data (SULEICA) available, and we feel that the isotropic pressure is well determined. (A more accurate description would use anisotropic pressure ($p_\perp \neq p_\parallel$), but anisotropic pressure values for AMPTE/IRM are not currently available.) For these two events, poloidal and compressional waves do occur in regions of a dip in poloidal frequency (Figures 2h and 4h) in agreement with the *Vetoulis and Chen* [1994, 1996] theory. The observed frequencies are also in rough agreement with the theoretical frequencies, if one allows that some waves may have higher harmonic parallel structure (4th harmonic in the case of the third wave event observed on 26 July 1986).

[32] For these two events the pressure is not greatly changed if we drop the high-energy component, but there can be some subtle differences in the L shell dependence. For instance, in the case of the 4 June 1985 event, the inclusion of the SULEICA data leads to a dip in square poloidal frequency, whereas without it, the poloidal frequency is flatter with respect to L. On the basis of this observation we would hope that without the SULEICA data, we would at least have a rough estimate of the theoretical frequencies.

[33] For the 17 May 1985 and 6 June 1985 wave events, SULEICA data were not available. For one of these (17 May 1985), the observed poloidal wave has a frequency matching the third harmonic theoretical frequency (Figure 5h). For the other event (6 June 1985) the observed compressional frequencies do not match any of the theoretical frequencies. This may simply indicate that these compressional waves are on a different dispersion surface from the poloidal Alfven wave (though we must keep in mind that the observed pressure values may not be totally accurate).

[34] In conclusion, the observed poloidal oscillations appear to have frequencies which match the theoretical poloidal mode frequency. In order to come to this conclusion, however, some of the observed waves must be interpreted as higher harmonics than the second harmonic. The second harmonic is expected to be the most unstable [*Cheng and Lin*, 1987; *Chen and Hasegawa*, 1988, 1991; *Cheng and Qian*, 1994]. Furthermore, in the cases for which we have SULEICA particle data available, the observed oscillations appear in the vicinity of a dip in poloidal frequency. In the case of 17 May 1985 (for which we do not have SULEICA data) the theoretical poloidal frequency has a slight flattening with respect to L where the waves are observed. The compressional waves also occur in the region of a dip in poloidal frequency. In the case of 26 July 1986 the lowest compressional frequency measured is consistent with the theoretical poloidal frequency (it is above the minimum of the dip in the theoretical frequency), but for 6 June 1985 it is not.

[35] *Vetoulis and Chen* [1994, 1996] hypothesized that a dip in poloidal frequency would occur because of a sharp gradient in plasma pressure. However, as pointed out by *Denton and Vetoulis* [1998], the pressure profile must have a large second derivative with respect to L in order to lead to such a dip. (If there is a constant gradient in pressure, the poloidal frequency will be uniformly lowered with respect to the toroidal frequency as indicated by equation (2); the poloidal frequency needs to rise at larger L in order that there be a local minimum.) An example of such a pressure profile would be a step function, where the pressure drops precipitously from a constant value to zero. Vetoulis and Chen used such a pressure profile for their theoretical calculations. However, our results indicate that a dip in poloidal frequency may occur for other reasons. In the case of the 4 June 1985 poloidal wave event, the gradient in pressure causes the poloidal frequency to be reduced relative to the toroidal frequency, but it is the density profile that causes there to be a dip in poloidal frequency. The same is true for the 6 June 1985 compressional wave event. In the case of the 26 July 1986 compressional wave event, it appears that the L dependence of the magnetic field may play a role in creating a dip in poloidal frequency.

[36] The density and magnetic field contribute to the frequency through the dependence of the poloidal frequency on the Alfvén speed. Neglecting the pressure term in equation (2), $\omega \sim k_\parallel V_A \sim B/\left(L\sqrt{n_e}\right) \sim L^{-4}/\sqrt{n_e}$ in a dipole magnetic field. Typically in the plasmatrough $n_e \propto L^{-4.5}$ [*Carpenter and Anderson*, 1992], so that $\omega \sim L^{-1.75}$ decreases with respect to L (the frequency also typically decreases in the plasmasphere). In order to have a dip in poloidal frequency, the frequency must increase at some location. Such an increase can be caused by a precipitous drop in density, leading to an increase in V_A. That is what occurs, for instance, in Figure 2 (see Figures 2e and 2h). Such a sudden decrease in density also typically occurs at the plasmapause, and this could provide an explanation for poloidal modes observed at that location.

[37] **Acknowledgments.** We especially thank the IRM magnetometer team (H. Lühr), plasma instrument team (G. Paschmann), plasma wave instrument team (B. Häusler), and SULEICA team (E. Möbius). We also thank the following for making data available on the web: NSSDC for NOAA data on OMNIWeb, A. Szabo and R. P. Lepping for high-resolution IMP-8 magnetometer data, the Danish Meteorological Institute for Greenland magnetometer data, and the institutes maintaining the IMAGE magnetometer array for EISCAT magnetometer data. Jim LaBelle provided important input to the interpretation of the IRM plasma wave data and we thank Mary Hudson for useful conversations. Work at Dartmouth was supported by NSF grant ATM-9911975 and NASA Sun-Earth Connection Theory Program grant NAG5-11735. A referee contributed to the material in the last paragraph of the paper.

[38] Lou-Chuang Lee thanks Liu Chen and Ian R. Mann for their assistance in evaluating this paper.

References

Anderson, B. J., Statistical studies of Pc 3–5 pulsations and their relevance for possible source mechanisms of ULF waves, *Ann. Geophys.*, *11*, 128, 1993.

Carpenter, D. L., and R. R. Anderson, An ISEE/whistler model of equatorial electron density in the magnetosphere, *J. Geophys. Res.*, *97*, 1097, 1992.

Chan, A., Interaction of energetic ring current protons with magnetospheric hydromagnetic waves, Ph.D. thesis, Princeton Univ., Princeton, N. J., 1991.

Chen, L., and A. Hasegawa, On magnetospheric hydromagnetic waves excited by energetic ring current particles, *J. Geophys. Res.*, *93*, 8763, 1988.

Chen, L., and A. Hasegawa, Kinetic theory of geomagnetic pulsations, 1, Internal excitations by energetic particles, *J. Geophys. Res.*, *96*, 1503, 1991.

Cheng, C. Z., and C. S. Lin, Eigenmode analysis of compressional waves in the magnetosphere, *Geophys. Res. Lett.*, *14*, 884, 1987.

Cheng, C. Z., and Q. Qian, Theory of ballooning mirror instabilities for anisotropic pressure plasmas in the magnetosphere, *J. Geophys. Res.*, *99*, 11,193, 1994.

Denton, R. E., Compressibility of the poloidal mode, *J. Geophys. Res.*, *103*, 4755, 1998.

Denton, R. E., and G. Vetoulis, Global poloidal mode, *J. Geophys. Res.*, *103*, 6729, 1998.

Ding, D. Q., R. E. Denton, M. K. Hudson, and R. L. Lysak, An MHD simulation study of the poloidal mode field line resonance in the Earth's dipole magnetosphere, *J. Geophys. Res.*, *100*, 63, 1995.

Goldstein, J., R. E. Denton, M. K. Hudson, E. G. Miftakhova, S. L. Young, J. D. Menietti, and D. L. Gallagher, Latitudinal density dependence of magnetic field lines inferred from Polar plasma wave data, *J. Geophys. Res.*, *106*, 6195, 2001.

Häusler, B., et al., The plasma wave instrument onboard the AMPTE IRM satellite, *IEEE Trans. Geosci. Remote Sens.*, *GE-23*, 267, 1985.

Li, X., H. R. Lewis, J. LaBelle, T.-D. Phan, and R. A. Treumann, Characteristics of the ion pressure tensor in the Earth's magnetosheath, *Geophys. Res. Lett.*, *22*, 667, 1995.

Lühr, H., N. Klöcker, W. Oelschlägel, B. Häusler, M. Acuna, *IEEE Trans. Geosci. Remote Sens.*, *GE-23*, 259, 1985.

Mann, I. R., and G. Chisham, Comment on "Concerning the generation of geomagnetic giant pulsations by drift-bounce resonance ring current instabilities" by K.-H. Glassmeier et al., *Ann. Geophys.*, *18*, 161, 2000.

Mann, I. R., and A. N. Wright, Finite lifetimes of ideal poloidal Alfvén waves, *J. Geophys. Res.*, *100*, 23,677, 1995.

Möbius, E., et al., The time-of-flight spectrometer SULEICA for ions of the energy range 5–270 keV/charge on AMPTE IRM, *IEEE Trans. Geosci. Remote Sens.*, *GE-23*, 274, 1985.

Paschmann, G., H. Loidl, P. Obermayer, M. Ertl, R. Laborenz, N. Sckopke, W. Baumjohann, C. W. Carlson, and D. W. Curtis, The plasma instrument for AMPTE IRM, *IEEE Trans. Geosci. Remote Sens.*, *GE-23*, 262, 1985.

Paschmann, G., I. Papamastorakis, W. Baumjohann, N. Sckopke, C. W. Carlson, B. U. Ö. Sonnerup, and H. Lühr, The magnetopause for large magnetic shear: AMPTE/IRM observations, *J. Geophys. Res.*, *91*, 11,099, 1986.

Southwood, D. J., A general approach to low-frequency instability in the ring current plasma, *J. Geophys. Res.*, *81*, 3340, 1976.

Takahashi, K., J. F. Fennell, E. Amata, and P. R. Higbie, Field-aligned structure of the storm time Pc 5 wave of November 14–15, 1979, *J. Geophys. Res.*, *92*, 5857, 1987.

Takahashi, K., R. E. Denton, and D. L. Gallagher, Toroidal wave frequency at L = 6–10: AMPTE/CCE observation and comparison with theoretical model, *J. Geophys. Res.*, *107*(A2), 1020, doi:10.1029/2001JA000197, 2002.

Vetoulis, G., and L. Chen, Global structures of Alfvén-ballooning modes in magnetospheric plasmas, *Geophys. Res. Lett.*, *21*, 2091, 1994.

Vetoulis, G., and L. Chen, Kinetic theory of geomagnetic pulsations, 3, Global analysis of drift Alfvén ballooning modes, *J. Geophys. Res.*, *101*, 15,441, 1996.

R. E. Denton, Department of Physics and Astronomy, 6127 Wilder Laboratory, Dartmouth College, Hanover, NH 03755, USA. (richard.denton@dartmouth.edu)

L. M. Kistler, Space Science Center, Morse Hall, University of New Hampshire, Durham, NH 03824-3525, USA. (lynn.kistler@unh.edu)

M. R. Lessard, Thayer School of Engineering, Dartmouth College, HB 8000, Hanover, NH 03755, USA. (marc.lessard@dartmouth.edu)